Challenges and Perspectives of the Phase Formation of Internally Oxidized PIT-Type Nb_3Sn Conductors

Carl Buehler , Bernd Sailer, Matheus Wanior , Vital Abaecherli, Manfred Thoener, Klaus Schlenga, Sandra Kauffmann-Weiss , Jens Hänisch , Martin Heilmaier, and Bernhard Holzapfel

Abstract—**Promising results of internally oxidized conductors based on Bruker's Powder-In-Tube (PIT) design are presented. SnO_2 was used as an oxygen source and Nb1Zr/Nb2.5Ti were chosen as the Nb alloy precursor. At a reduced field of $B/B_{c2} = 0.5$, an increase of more than 70 % in non-Cu J_c against a standard PIT reference was measured. No correlation between oxygen content of the conductor core and grain size was observed. The performance increase was attributed to nanoscale precipitates that act as APC's and lead to an increased point pinning component in the internally oxidized samples. The lack of grain refinement is seen as the result of the formation of Nb-Sn intermetallics prior to the oxygen release and Nb_3Sn formation that inhibit an adequate oxygen supply to the Nb alloy.**

Index Terms—**Multifilamentary superconductors, Niobium-tin, Critical current density, Flux pinning.**

I. INTRODUCTION

CURRENT superconducting wires based on Nb_3Sn require a significant improvement in J_c performance to fulfill the challenging target specifications of the Future Circular Collider (FCC): A non-Cu J_c of 1500 A/mm² at 16 T (or approximately 3500 A/mm² at 12 T each at 4.2 K) [1]. With the critical current density of a conductor being inversely proportional to the Nb_3Sn grain size [2], [3], one promising possibility to improve the material's performance lies in refining its grain size. In 1982 Jergelt *et al.* [4] showed that the internal oxidation of a Nb1.5Zr alloy leads to grain refinement and a 200% increase of the critical current density for tape-shaped samples. Rumaner and Benz demonstrated in 1994 that the internal oxidation of a Nb-Zr alloy in Nb-foil-based diffusion-couples prior to the Nb-Sn phase formation results in dispersed, oxidic precipitates that significantly reduce Nb_3Sn grain growth [2]. The grain size was refined from 2–3 μm to 200–500 nm. In 2014 Xu *et al.* [5] resumed the topic for multifilamentary conductors from Zeitlin *et al.* [6] by placing an oxygen source concentrically between the central Sn

source and the surrounding Nb-alloy in a tube tube-type design. With oxygen supplied from SnO_2, they observed a $J_{c\text{-layer}}$ of 9600 A/mm² at 12 T and grain sizes of 36 to 43 nm using a Nb1Zr alloy (at 650 °C and 625 °C respectively) [7]. While first studies on multifilamentary conductors were based on filaments with separated Sn and oxygen sources [7], more recent publications on multifilamentary conductors focus on designs with mixed cores containing Sn and O in one central location [8], [9]. In such wires, the oxidation of the Nb alloy precursor and the Sn diffusion are not fully separated. These designs do not show the same degree of grain refinement initially observed (70–80 nm [8] instead of 20–50 nm [7]). Recent impressive reports show that they can, nonetheless, achieve the FCC target-specification [9].

The present report investigates the phase formation and performance of internally oxidized PIT conductors with the goal to better understand the following key points:

- Which aberrations from the standard phase formation of oxygen-free PIT conductors are induced and how can they be used to increase the conductor's performance?
- When are nano-scale precipitates formed and can they lead to a grain refinement in concepts with an oxygen- and tin-rich, mixed core?
- Can such precipitates act as Artificial Pinning Centers (APCs) that improve the in-field properties?

In this paper, filament designs that feature a central tin- and oxygen-rich mixed core are investigated. Based on the results of these layouts, conclusions for future, improved conductor designs are drawn.

II. MATERIALS AND METHODS

Filaments for the internal oxidation are based on a Nb 2.5wt% Ti and Nb 1wt% Zr alloy tubes filled with a central powder core surrounded by a 1–2 μm thin Cu liner. The powder contains an oxygen source in the form of SnO_2 as well as tin-rich powders of various compositions. As a first step, the phase formation of 20 different compositions was investigated in screening conductors that are not suitable for current density measurements.

A selection of the most promising compositions was used to manufacture four R&D conductors with 32 hexagonal 47 μm filaments. These conductors only carry a comparatively small amount of superconducting material so that the critical current density can be measured down to 1T. As a reference, a standard

Name	Alloy Type in wt%	Oxygen Content
A	Nb1Zr	Low
B	Nb1Zr	Medium
C	Nb1Zr	High
D	Nb2.5Ti	High
PIT Ref.	Nb7.5Ta	-

Ta-doped 192 filament PIT global barrier conductor with round 40 μm filaments was used. This way, the inscribed circle within each hexagonal filament ($\sim$43 μm), that sets the limit for an outward Sn-diffusion, approximates the diameter in the round sample.

All oxygen contents within the cores are sufficient to fully oxidize the Zr in the Nb1Zr alloy tube. For the Nb2.5Ti alloy, ideally, unreacted Ti remains in the alloy to increase B_{c2}. All compositions are listed in Table I.

Three representative heat treatments were chosen:

- HT-1: 300 h at 640 °C with a heating rate of 30 K/h as a reference.
- HT-2: 300 h at 640 °C with a fast heating rate of 330 K/h to avoid as much formation of Nb-Sn intermetallics as possible before the bulk of Nb_3Sn forms.
- HT-3: Similar to HT-1 but features an additional, intermediate 300 h dwell at 500 °C with the goal to promote oxygen diffusion at low temperatures.

All heat treatments have the same high temperature stage in order to rule out the influence of reaction temperature and time on the A15 grain size [10].

The Nb_3Sn grain size was defined as follows: Secondary electron images of fracture surfaces were obtained using a ZEISS Sigma 300 Field Emission Scanning Electron Microscope (FE-SEM) at a FOV of 1.505 μm, a 30 μm aperture and 15 kV acceleration voltage. The outline of each visible grain was traced on transparent foil by hand. The tracing was scanned at 600 dpi and then segmented and cleaned up by a fixed set of predefined editing steps using MIPAR [11]. Subsequently, the line width of the selection was reduced to 1 px after which the grain size was measured as the average equivalent diameter d_{eq} of each grain (Fig. 1(a)).

Electrical transport properties were measured on standard TiAlV mandrels at 4.2 K from 18 to 1 T using a 0.1 μVcm^{-1} criterion. For oxygen free samples B_{c2} was determined by means of a Kramer extrapolation from 6 T to 18 T using $p = 0.5$ and $q = 2$. As additional point pinning components were expected for the oxidized samples [12], their B_{c2} was measured by determining the parameters A, B and B_{c2} in $F_p \sim A\ c \cdot b^{0.5}(1-b)^2 + B \cdot b(1-b)^2$ [13] with $b = B/B_{c2}$. From A and B, the point defect (PD) and grain boundary (GB) contributions to the pinning force density were calculated.

III. RESULTS

A. Morphological Analysis

As shown in Fig. 1(b), no significant grain refinement could be measured against the PIT reference for HT-1 to 3 and no
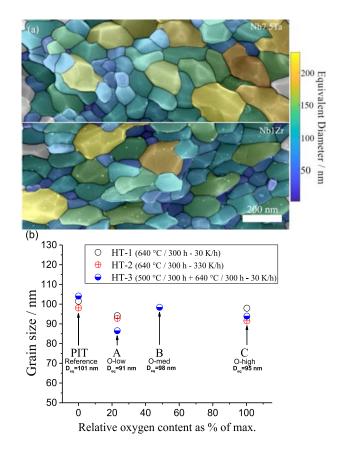

Fig. 1. (a) Fracture surfaces of Nb_3Sn of heat treatment HT-3 including original tracing. The size of each grain is indicated by coloring it according to its d_{eq} determined after segmentation. (Top) Average Grain Size obtained from Nb7.5Ta: 104 nm. (Bottom) Average Grain size obtained from Nb1Zr: 94 nm. The surface of the grain boundaries in the oxidized sample is decorated with nanoscale precipitates. (b) Grain Sizes from the Nb1Zr alloy for different core compositions at HT-1 to 3 plotted against the oxygen content relative to the maximum amount of oxygen within a core. No oxygen-induced grain refinement was observed in any heat treatment. Grain sizes for the Nb2.5Ti sample (not shown) are comparable to the Nb1Zr samples.

correlation between oxygen content and grain size was observed. Presumably, for a conductor layout with a mixed central oxygen and tin source, none of the heat treatments supplied sufficient oxygen to the unreacted Nb alloy precursor prior to the Nb_3Sn formation to refine the A15 grain size. However, nano-scale precipitates of $\sim$5–7 nm diameter were observed on grain boundary surfaces of oxidized samples. Similar findings were reported in ref. [12]. By SEM, no precipitates were visible on transcrystalline fracture surfaces. Preliminary TEM results indicate that these precipitates are the oxides of the respective alloying element.

To understand further why no grain refinement occurred, the phase formation of the oxygen-rich Nb2.5Ti-based sample D was compared to an oxygen-free reference sample during the heat treatment (Fig. 2). The following heat treatments were chosen: P1: 230 °C/40 h + 415 °C/40 h (the peritectic decomposition of η-bronze); P2: 500 °C/300h (to assess $NbSn_2$-formation) and P3: P1 + 625 °C/40 h (at the beginning of the Nb_3Sn formation). As an example for a fully reacted filament, HT-1 with 640 °C/300 h was included.
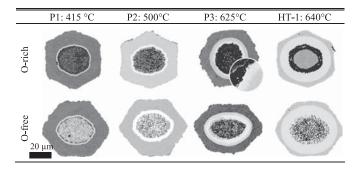
Fig. 2. BSE images of cross-sections of reacted 47 μm filaments depicting the phase development during heat treatment of Nb2.5Ti samples with a high oxygen content (top) and an oxygen-free core (bottom). Below 500 °C no signs for an oxidation reaction are visible. Above 625 °C, the oxidation of Nb_6Sn_5 occurs. At 640 °C, a dark oxide ring surrounds the O-rich filament. The reference shows significantly higher coarse-grain and core A15 fractions.
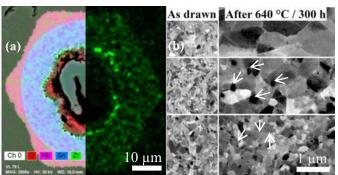

Fig. 3. (a) EDX mapping of an oxidized Nb1Zr filament including the overlay of the elements Nb, Sn, O and Zr on a BSE image and the pure element mapping of Zr. An inner oxidic ring as well as the accumulation Zr in the form of ZrO_2 are visible at the interface between oxide ring and Nb_3Sn as a bright green circle line. Similar observations were made from Nb2.5Ti. (b) Morphology of the unreacted Nb-alloy. Left after drawing, right remaining on the outside of a filament after 300 h at 640 °C. From top to bottom Former Nb7.5Ta alloy, Nb2.5Ti alloy, Nb1Zr alloy. All alloys show a recrystallized structure. Significant grain refinement is visible in the Zr-alloy. For the –Ti and –Zr alloys precipitation of the respective alloying element (measured by EDX) can be seen as dark, partially diffuse areas (exemplary precipitates marked with arrows). No increase in oxygen levels could be determined by EDX in these areas.

After 40h at 415 °C, a homogeneous bronze spans throughout the core, encasing the so far unaltered core components. An approx. 1 μm thick layer of bright Nausite (determined by EDX) lines the inner side of the alloy tube. This is similar to results from ref. [14]–[17]. After 300 h at 500 °C, the Nausite has decomposed and a more than 2.5 μm thick layer of $NbSn_2$ expands into the Nb-precursor. It appears to be in equilibrium with a 25 at% Sn bronze. Between 500 and 625 °C, an inner layer of Nb_6Sn_5 has formed from the decomposition of $NbSn_2$ and the outward diffusion of tin. Radially outward, fine-grain Nb_3Sn is growing and in some occasions (not depicted) the nucleation of coarse-grain Nb_3Sn at the interface of Nb_6Sn_5 and Nb_3Sn can be seen. For the O-rich sample, the first signs of an oxidation reaction appear in this temperature range, visible as darkened, convex areas that reach outward into the Nb_6Sn_5 layer. This is consistent with Xu *et al.* who observed the formation of Nb-oxides above 550 °C from a Nb-alloy precursor that was in direct contact with SnO_2 powder [5]. After the full reaction in HT-1 (640 °C/300 h), the reference core is filled with the decomposition products of the core embedded in a depleted bronze, whereas the oxidized sample segregates into a central depleted bronze droplet surrounded by an oxide ring. This bronze core can deplete down to 4 at% Sn for the Nb1Zr-based conductors showing that the oxide ring is permeable to Sn. EDX measurements show that this ring consists of a mixture of Nb_2O_5 and NbO_2 as well as oxides of the respective alloying element (Fig. 3(a)). It must therefore form by oxidizing intermediary Nb-Sn intermetallics as visible in P3. If left un-oxidized, these compounds eventually form a coarse grain layer of Nb_3Sn that does not contribute to the transport current but retains about 1/4 of the Sn that is available for the Nb_3Sn formation [17]. When oxidized, little to no precursor material for the formation of coarse-grain A15 remains. Measurements of the fine-grain Nb_3Sn fraction confirm this by showing that O-rich samples can form the same amount of fine-grain Nb_3Sn as the standard PIT sample (40% to 42% for HT-1 to 3) even though their absolute Sn content is lower. At the interface between oxide ring and Nb_3Sn, a local increase of Zr or Ti respectively can be observed. Presumably, some of the alloying element is expelled from the forming Nb_3Sn. It subsequently either diffuses towards the core where

it is oxidized or outward into the still unreacted Nb-alloy. This way the Nb_3Sn phase boundary pushes a growing concentration front of the alloying element forward into the Nb alloy until the solubility limit of the alloying element is exceeded and either Zr or Ti precipitates are formed. An example for this process is depicted in Fig. 3(b). After 300 h at 640 °C, all remaining Nb alloys have recrystallized but a significantly refined grain size is visible for Nb1Zr. This is attributed to the formation of smaller, more homogeneously distributed precipitates that result in more effective Zener pinning of the grain boundaries. No correlation between grain size of the recrystallized Nb alloy and the Nb_3Sn grain size could be observed.

B. Pinning Properties

Non-Cu J_c measurements (insert in Fig. 4(a)) from 1 to 18 T show that the Nb1Zr-based, oxygen rich sample C can already achieve standard PIT performance below fields of approximately 10 to 12 T in HT-2 and HT-3 which is astonishing given hexagonal filament structure. Above the field region of 10–12 T, the lack of Ta doping leads to a significantly faster J_c deterioration relative to the PIT sample. No detrimental effect of oxygen on B_{c2} was observed. Kramer extrapolation resulted in $B_{c2} =$ 21.1 T for the oxidized and 26.8 T for the PIT standard samples. No significant influence of the heat treatment on oxidized or regular PIT conductors could be measured. Exemplary depicted for HT-3, the oxygen-poor sample A drastically underperforms the samples with higher oxygen contents. For the sake of clarity, the Nb2.5Ti sample was omitted, its performance is slightly lower than the Nb1Zr samples' at medium and high oxygen concentrations.

To compare the performance of oxidized samples with the PIT reference, the data for sample C are plotted against the reduced field $b = B/B_{c2}$ in the main plot of Figure 4. All oxidized samples show a significant improvement over the PIT
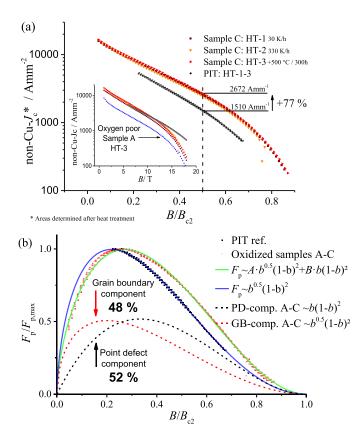
Fig. 4. (a) non-Cu J_c plotted against the reduced field B/B_{c2} for all Nb1Zr based, oxidized samples with a high oxygen content as well as a PIT reference. Three different heat treatments are depicted: HT-1: 640 °C/300 h, 30 K/h; HT-2 640 °C/300 h, 330 K/h; HT-3: 500 °C/300 h, 640 °C/300 h 30 K/h. The Insert shows the non-Cu-J_c of the same samples against the applied field. Up to 10–12 T the oxidized samples outperform the PIT counterpart despite their lack of Ta doping. (b) Normalized pinning force density ($F_p/F_{p,max}$) curves for all Nb1Zr samples with low medium and high oxygen contents compared to the standard PIT reference in HT-1 to 3 and according fits. All oxidized samples converge into one curve. Dashed curves indicate point and grain boundary pinning components for the averaged oxidized results. Measurements performed in liquid helium at 4.2 K with the Lorenz force radially inward.

reference. At $b = 0.5$, HT-3 has a 77% increased non-Cu J_c compared to the PIT sample. To understand the origin of this performance improvement, the normalized pinning force density of the oxidized Nb1Zr based and reference samples was plotted against the reduced field for HT-1 to 3 (Fig. 4(b)). The oxidized samples converge into a single curve that can be clearly distinguished from the standard PIT reference by an increased pinning component at higher fields. The location of the maximum of this curve is shifted from $b = 0.20$ in the PIT reference to $b = 0.26$ for the oxidized samples. The grain boundary- and point-pinning components for the oxidized samples were separately fitted. A point defect contribution of 52% was calculated for the Nb1Zr-based oxidized samples, which is slightly lower than the 65–76% reported by Motowidlo et al. [12] indicating that their mixed η-bronze / SnO_2 core could have supplied more oxygen to the Nb-alloy, possibly by retarding the tin release compared to a core with low melting elemental tin. Despite the higher amount of alloying element, the Nb2.5Ti based samples show a reduced PD contribution of only 38%.

Due to the observed limited solubility of the alloying elements in the formed Nb_3Sn, it appears likely that the amount of precipitates responsible for the increased PD contribution is determined by the solubility and mobility of the alloying element in the A15 phase. Accordingly, increasing the amount of alloying element is not expected to lead to significantly more precipitates in designs with a mixed tin and oxygen source.

The shift of the pinning force maximum, the increased point pinning component as well as the convergence of all pinning force density curves of oxidized conductors clearly point to an additional pinning mechanism in these samples. As no significant reduction in grain size could be observed, it is assumed that this additional pinning component is caused by the previously described nano-scale precipitates. If additional Ta doping can increase B_{c2} of this design to the level of a standard PIT conductor as recent reports demonstrated [9], the impact of the generated precipitates would suffice to achieve the FCC specification.

IV. CONCLUSION

As demonstrated, conductor concepts featuring a central oxygen- and tin-rich core encased with a Cu liner have the potential to improve the performance of Brukers PIT conductors beyond the FCC specification. In detail, we showed:

- The addition of SnO_2 to a filament core leads to the oxidation of Nb-Sn intermetallics which sets in between 500 and 625 °C. This reaction can be used to release Sn that would otherwise remain bound in coarse grain- or core-Nb_3Sn that does not contribute to the superconducting transport current. Indications were found that these intermetallics impede the internal oxidation of the Nb-alloy.
- Nano-scale precipitates can be generated most likely only after the start of the Nb_3Sn formation. Therefore, no grain refinement can occur. The amount of precipitates that can be formed is therefore limited by the solubility of the alloying element in the A15 phase.
- Compared to a standard PIT conductor, oxidized conductors show an additional pinning component at higher fields. Plausibly, this is due to precipitates acting as artificial pinning centers. A shift of the maximum pinning force density from 0.20 to 0.26 was observed.
- At a reduced field of $B/B_{c2} = 0.5$, a 77% increase in non-Cu J_c was observed for the samples with the highest oxygen content compared to the PIT-reference sample.

Future work will address the generation of APCs in Nb-Zr-Ta alloys. New conductor concepts based on a separated Sn and oxygen diffusion are planned. These designs aim at mitigating the formation of Nb-Sn intermetallics so that an early internal oxidation of the Nb-alloy can be achieved.

REFERENCES

[1] A. Ballarino, The CERN FCC Conductor Program, FCC Week 2017, Berlin, 2017. [Online]. Available: https://indico.cern.ch/event/556692/contributions/2591608/attachments/1467217/2268687/Ballarino_1.pdf
[2] L. E. Rumaner and M. G. Benz, "Effect of oxygen and zirconium on the growth and superconducting properties of Nb_3Sn," *Metallurgical Mater. Trans. A*, vol. 25, no. 1, pp. 203–212, 1994.
[3] X. Xu, "A review and prospects for Nb_3Sn superconductor development," *Supercond. Sci. Technol.*, vol. 30, no. 9, 2017, Art. no. 93001.

[4] M. Jergelt, "Influence of oxygen content on some properties of Nb_3Sn tape used for superconducting transmission lines," *J. Mater. Sci.*, vol. 17, pp. 1579–1584, 1982.

[5] X. Xu, "Refinement of Nb_3Sn grain size by the generation of ZrO_2 precipitates in Nb_3Sn wires," *Appl. Phys. Lett.*, vol. 104, no. 9, 2014, Art. no. 082602.

[6] B. A. Zeitlin *et al.*, "Results on mono element internal tin Nb_3Sn conductors (MEIT) with Nb7.5Ta and Nb(1 Zr + Ox) filaments," *IEEE Trans. Appl. Supercond.*, vol. 15, no. 2, pp. 3393–3398, Jun. 2005.

[7] X. Xu, M. D. Sumption, and X. Peng, "Internally oxidized Nb_3Sn strands with fine grain site and high critical current density," *Adv. Mater.*, no. 27, pp. 1346–1350, 2015.

[8] X. Xu, J. Rochester, X. Peng, M. Sumption, and M. Tomsic, "Ternary Nb_3Sn superconductors with artificial pinning centers and high upper critical fields," *Supercond. Sci. Technol.*, vol. 32, no. 2, 2019, Art. no. LT01.

[9] X. Xu, X. Peng, J. Rochester, M. Sumption, and M. Tomsic, "Achievement of FCC specification in critical current density for Nb_3Sn superconductors with artificial pinning centers," 2019, *arXiv1903.08121*.

[10] C. D. Hawes, P. J. Lee, and D. C. Larbalestier, "Measurements of the microstructural, microchemical, and transition temperature gradients of A15 layers in a high-performance Nb_3Sn powder-in-tube superconducting strand," *Supercond. Sci. Technol.*, vol. 19, no. 3, pp. S27–S37, 2006.

[11] J. M. Sosa, D. E. Huber, B. Welk, and H. L. Fraser, "Development and application of MIPAR: A novel software package for two- and three-dimensional microstructural characterization," *Integrating Mater. Manuf. Innov.*, vol. 3, pp. 123–140, 2014.

[12] L. R Motowidlo *et al.*, "An intermetallic powder-in-tube approach to increased flux-pinning in Nb_3Sn by internal oxidation of Zr," *Supercond. Sci. Technol.*, vol. 31, 2018, Art. no. 014002.

[13] T. Baumgartner, "Performance boost in industrial multifilamentary Nb_3Sn wires due to radiation induced pinning centers," *Sci. Rep.*, vol. 5, Art. no. 10236, 2015.

[14] C. Sanabria, "A new understanding of the heat treatment of Nb-Sn superconducting wires," Ph.D. dissertation, Florida State Univ., 2017.

[15] S. Martin *et al.*, "The crystal structure of $(Nb_{0.75}Cu_{0.25})Sn_2$ in the Cu-Nb-Sn system," *Intermetallics*, vol. 80, pp. 16–21, 2017.

[16] M. Di Michiel and C. Scheuerlein, "Phase transformations during the reaction heat treatment of powder-in-tube Nb_3Sn superconductors," *Supercond. Sci. Technol.*, vol. 20, no. 10, pp. L55–L58, 2007.

[17] C. Segal, C. Tarantini, P. Lee, and D. C. Larbalestier, "Improvement of small to large grain A15 ratio in Nb_3Sn PIT wires by inverted multistage heat treatments," *IOP Conf. Ser.: Mater. Sci. Eng.*, vol. 279, 2007, Art. no. 012019.